ELSEVIER

Polymer 42 (2001) 3043–3055

polymer

www.elsevier.nl/locate/polymer

Temperature dependence of the fracture behavior of nylon 6/ABS blends

T.G. Pressly, H. Keskkula, D.R. Paul*

Department of Chemical Engineering and Texas Materials Institute, The University of Texas at Austin, Austin, TX 78712, USA

Received 30 June 2000; received in revised form 5 September 2000; accepted 14 September 2000

Abstract

Essential work of fracture and critical strain energy release rate analyses were used to investigate the effect of temperature (from 25 to −25°C) and specimen ligament length on the fracture energy, obtained from an instrumented drop tower test, of two compatibilized nylon 6/ABS blends (40 and 25 wt% ABS) and the neat ABS. Three types of fracture were observed: ductile, mixed mode, and brittle. The essential work of fracture parameters were obtained by an analysis of the fracture energies for samples that failed in a ductile manner. The dissipative energy density, u_d, was found to decrease with decreasing temperature for each of the three materials, while the specific limiting fracture energy, u_o, was found to be nearly invariant with temperature for the two blends but to decrease with decreasing temperature for the ABS. The critical strain energy release rate, G_{IC}, model gives an excellent description of the fracture energies of samples that failed in a brittle manner; G_{IC} was found to decrease as temperature was reduced. The yield stress, σ_y, and the plane-strain critical stress intensity factor, K_{IC}, were also determined. The yield stress was found to be invariant with temperature, while K_{IC} decreases as the temperature is lowered.

Keywords: Nylon 6; ABS; Fracture

1. Introduction

A number of approaches for achieving super tough materials by blending nylon 6 with poly(acrylonitrile-butadiene-styrene) (ABS) and appropriate compatibilizers have been reported in the literature [1–12]. The choice of the ABS and the compatibilizing polymer is critical for achieving a composite material with superior toughness over a wide range of temperatures. The compatibilizer serves to improve the dispersion of the ABS phase and to bond it to the polyamide matrix. The rubber particles in the ABS phase cavitate during the fracture process permitting shear yielding of the polyamide matrix, which leads to the superior toughness. Ductile fracture by this mechanism occurs over a wide temperature range leading to the low ductile–brittle transition temperatures that are useful in a number of large scale applications.

The purpose of this paper is to examine the details affecting the ductile–brittle transition of compatibilized nylon 6/ABS blends. Fracture resistance is measured by a single edge notched three point bend test, using a drop tower, from which load–displacement data are recorded. In contrast with an Izod test, samples are typically fractured almost completely with only a hinge remaining. In addition, variable ligament lengths and thick specimens with sharp notches are used. These differences allow the ductile–brittle transition in these materials (neat ABS, and blends with 40 and 25 wt% ABS) to be analyzed thoroughly and compared to the ductile–brittle transition temperature obtained from the Izod test. The essential work of fracture and the yield stress models are used to study the effect of temperature on the fracture energies and failure stresses from the samples which fail in a ductile manner. Likewise, the critical strain energy release rate, G_{IC}, and the critical stress intensity factor, K_{IC}, models are used to interpret the fracture energies and failure stresses as a function of temperature from those specimens which fail in a brittle manner.

1.1. Background: essential work of fracture, G_{IC}, yield stress, and K_{IC}

The essential work of fracture (EWF) method originated with Broberg [13]. It is a method of quantifying the relative contributing effects in fracture [12,14–28]. In this analysis, fracture is modeled as consisting of two zones: (a) an elastic zone in which the initiation and propagation of the crack occurs and (b) a surrounding plastic zone in which energy is absorbed by plastic deformation during the crack extension. Mai and coworkers used this theory to divide the total fracture energy (W_f) into W_e, the essential work or energy

* Corresponding author. Tel.: +1-512-471-5392; fax: +1-512-471-0542.
E-mail address: drp@che.utexas.edu (D.R. Paul).

0032-3861/01/$ - see front matter
PII: S0032-3861(00)00696-0

associated with the crack initiation and extension, and W_p, the non-essential plastic work or the energy associated with the plastic deformation in the region surrounding the crack [16,19,29,30]:

$$W_f = W_e + W_p \tag{1}$$

They propose the following equation based on the assumptions that W_e is proportional to the fracture area and W_p is proportional to the volume of the plastic zone [16,19,29,30]:

$$w_f = w_e + \beta l w_p \tag{2}$$

where, w_f is the specific fracture energy, w_e is the specific essential work of fracture, β is a shape factor, l is the ligament length, and w_p is the specific non-essential plastic work. This model has the requirements that a ligament must be fully yielded before fracture and has the following limitation on the ligament length:

$$5t < l < \min(W/3, 2r_p) \tag{3}$$

where t is the sample thickness, W is the width, and r_p is the size of the plastic zone. A similar model for the specific energy was also proposed by Vu Khanh:

$$\frac{U}{A} = G_i + \tfrac{1}{2} A T_a \tag{4}$$

where U is the total energy of fracture, A is the area of the fracture (lt), G_i is called the fracture energy at crack initiation, and T_a is claimed to be a tearing modulus [14]. A previous study of nylon 6/ABS blends using samples of varying thickness has shown that the approach by Mai is more appropriate for the materials used in this work, since the second term was found to be better described by the ligament length than the ligament area [12].

Because the yielding and the ligament length size criteria of the EWF methodology as proposed by Mai and coworkers may not always be satisfied in this study, a different nomenclature is used in this and previous papers employing similar conditions [12]:

$$\frac{U}{A} = u_o + u_d l \tag{5}$$

The two parameters in this linear model are identified as follows: u_o is the limiting specific fracture energy and u_d is the dissipative energy density. Different ligament lengths are tested, with the result that a plot of U/A versus l has a slope of u_d and an intercept of u_o. Under appropriate conditions, $u_o = w_e$ and $u_d = \beta w_p$.

The critical strain energy release rate, G_{IC}, provides a similar analysis, but applying to the energy of brittle fractures [31,32]. The fracture energy at peak load is related to G_{IC} in the following manner:

$$U_{\text{peak load}} = U_K + G_{IC} t W \phi \tag{6}$$

where U_K is the kinetic energy required to accelerate a sample to the testing speed and ϕ is the energy calibration factor. The total energy of fracture was found to be essentially the same as the energy at peak load and is used instead. At the high testing rate used, the kinetic energy term, U_K, can represent a significant contribution to the total fracture energy for samples with short ligament lengths. The term ϕ is a function of ligament length or notch depth, a, and is given by the following for the specimen geometry used in this test:

$$\phi = \frac{A + 18.64}{dA/dx} \tag{7}$$

where x is a/W and A is as follows [32]:

$$A = \left(\frac{16x^2}{(1-x)^2}\right)(8.9 - 33.7x + 79.6x^2 - 113.0x^3 + 84.8x^4 - 25.7x^5) \tag{8}$$

Plane-strain conditions are necessary for this model and are expected only if the ratio of the notch depth to the width is less than or equal to 0.6. The ASTM testing standard also has the following size criterion to ensure plane-strain conditions [31]:

$$t, a, l > 2.5\left(\frac{K_{IC}}{\sigma_y}\right)^2 \tag{9}$$

where σ_y is the unnotched tensile yield stress at the same conditions as the fracture and $(K_{IC}/\sigma_y)^2$ is proportional to the size of the plastic zone around the crack tip. This criterion is satisfied for the thickness and ligament length, but may not always be satisfied for the notch depth, in this study. No correction is made for system compliance, tup penetration, and sample compression. The parameter G_{IC} is calculated as the slope from a plot of total fracture energy versus $tW\phi$; only data from samples failing in a brittle manner for which $a/W \leq 0.6$ were used in this analysis.

From load–displacement data, the stress at fracture can also be obtained [33]. The maximum tensile stress in an unnotched bar, σ_{max}, is given by the following relation from the theory of linear elasticity [34]:

$$\sigma_{max} = \frac{3SF}{2tW^2} \tag{10}$$

where S is the span, and F is the load at failure. This stress can be related to one of two parameters depending on whether the fracture is ductile or brittle. Using the net section argument, the failure stress for ductile fracture is related to the yield stress, σ_y:

$$\sigma_{max} = \sigma_y\left(\frac{W-a}{W}\right)^2 \tag{11}$$

For plane-strain brittle fracture, the fracture stress is given in terms of the critical stress intensity factor, K_{IC}, as follows:

$$\sigma_{max} = \frac{K_{IC}}{Y\sqrt{a}} \tag{12}$$

where Y is an empirically determined correlation, which is a

Table 1
Materials

Polymer	Description	Composition	Molecular weight	Source
Capron B73WP	Nylon 6	End-group content: NH2 = 47.9 μeq./g COOH = 43.0 μeq./g	$\bar{M}_n = 22,000$	AlliedSignal
SAN-g	Emulsion made ABS	45 wt% rubber 0.3 μm monodisperse rubber 25 wt% AN in SAN	$\bar{M}_n = 35,000$ $\bar{M}_w = 90,000$	Cheil Industries
IA	Imidized Acrylic (EXL 4140)	55.7 wt% methyl glutarimide 41.0 wt% methyl methacrylate 2.2 wt% methacrylic acid 1.1 wt% glutaric anhydride	$\bar{M}_w = 95,000$	Rohm and Haas

function of the sample geometry and the notch depth, and is as follows for the specimen geometry used here [35]:

$$Y = 1.93 - 3.07x + 14.53x^2 - 25.11x^3 + 25.80x^4 \quad (13)$$

The ASTM standard requires the use of a corrected stress in calculating K_{IC} [32]. However, this correction was found to be unnecessary for the conditions used in this study because failure occurred in the linear region of the stress-strain curve. Both the yield stress and the critical stress intensity factor are determined using non-linear regression analysis of plots of failure stress versus ligament length. In plane-strain, the values for K_{IC} and G_{IC} for the same material and testing conditions, in theory, are related as follows:

$$G_{IC} = \frac{(1 - \nu^2)K_{IC}^2}{E} \quad (14)$$

where ν is Poisson's ratio and E is the tensile modulus at the same testing conditions as the fracture test. At high testing rates, it is difficult to accurately determine the compliances, which will affect the calculation of G_{IC} and thus affect this relation [36].

In this study, the EWF methodology is applied to the analysis of only those samples which fractured in a ductile manner. The energies of the brittle fractures were found to be better represented by the critical strain energy release rate model, probably as a result of the criteria of the essential work of fracture model not being satisfied. By applying both of these models, the entire range of behavior is captured quantitatively. Similarly, by applying the models for the yield stress and the critical stress intensity factor, the failure stresses of samples failing both in a ductile manner and those failing in a brittle manner are analyzed.

2. Experimental

The materials used in this study are summarized in Table 1. The ABS (SAN-g) has a high rubber content (45 wt%) and generally would not be used neat as an engineering material, but only in blends. All compositions in this work are given in weight percent. The materials were dried at least 16 h. at 80°C in either a vacuum oven (for the nylon 6) or a convection oven (for the ABS and imidized acrylic polymer) prior to processing. The blends were prepared in a Killion single-screw extruder, with *L/D* of 30 and diameter of 2.54 cm, operated at 40 r.p.m. The extruder barrel temperature was set at 240°C. The resulting pellets were formed into test specimens by an Arburg Allrounder 305-210-700 injection molding machine (barrel temperature of 240°C, mold temperature of 65°C). Bars were molded into two thicknesses: 3.18 mm for Izod and 6.35 mm for drop tower tests. After molding, the materials were placed in a vacuum desiccator for at least 24 h prior to testing.

The notched Izod impact tests were conducted with a TMI tester (6.8 J hammer and 3.5 m/s impact velocity) using samples with a notch cut according to ASTM (radius = 0.25 mm) [37]. An instrumented Dynatup model 8200 drop tower with an attached computer for data acquisition was used for the three point bend tests; the data were recorded as load, or force, versus time. In each test, the tup velocity (approximately 3.4 m/s) was measured automatically just before the impact with the sample and was assumed constant during the fracture, which allowed displacement to be calculated. The fracture energy was determined from a numerical integration of the load–displacement data. The specimens were cut to 5.6 cm in length and prenotched at the center with a band saw. The tests were performed at a series of temperatures (25, 15, 5, −5, −15, and −25°C). At each temperature, 24 samples were tested; six different notch depths were used, with two gate and two far end samples for each depth. A fresh regular duty razor blade (0.23 mm thick) was tapped into the grove made by the band saw to create the sharp notch. The span of the supports in the test was 5.1 cm. The mass of the hammer was 14 kg (81 J capacity at the impact velocity).

The drop tower testing was conducted without any mechanical dampening for the neat ABS (SAN-g) and the blend containing 40 wt% ABS. A rubber pad (constructed from six layers of Safeskin latex rubber gloves) covering the tup and rubber bands securing the sample ends to the testing frame were used for mechanically dampening the vibrations

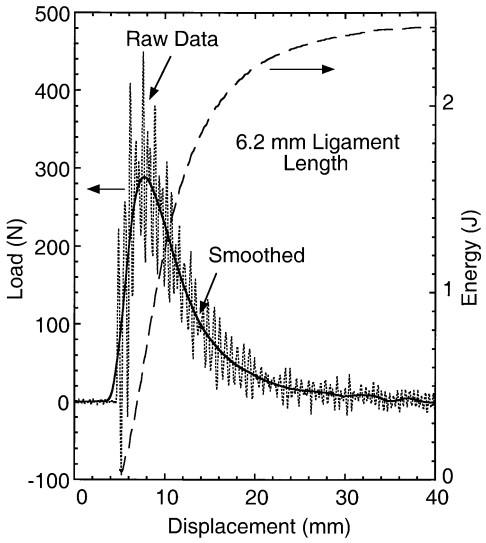

Fig. 1. Example of force-displacement data from a drop tower test for the 55/40/5 Capron B73WP/SAN-g/IA blend at 25°C with a 6.2 mm ligament length: raw data and smoothed data after Fourier analysis.

during testing of the 25 wt% ABS blend samples. One test was also performed on the 25 wt% ABS blend (at 25°C only) using no mechanical dampening for comparison.

A JEOL 200CX transmission electron microscope (TEM) at 120 kV was used to examine the blend morphology. Ultra-thin sections were cut using a Reichert-Jung Ultracut E microtome with the sample temperature set at −40°C. The sections were stained in a 2% aqueous solution of phosphotungstic acid, which makes the nylon phase appear as dark in the TEM images.

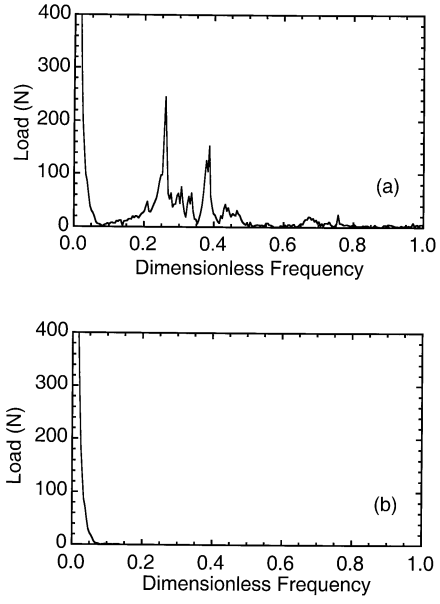

Fig. 2. (a) Magnitude of the Fourier transform of the raw data from Fig. 1. (b) Magnitude of the resulting smoothed data after a Gaussian kernel has been applied.

2.1. Smoothing techniques applied to the drop tower impact testing

The high velocity (3.4 m/s) at which the tup struck the samples causes vibrations in load to be recorded during the three point bend tests. Fig. 1 shows the raw and the smoothed data from the testing of a specimen, with a ligament length of 6.2 mm, composed of the 40 wt% ABS blend. The superposition of high frequency oscillations onto the load–displacement curves does not affect the total energy; however, it is difficult to determine the peak load or compare the results of two tests using these types of raw data. These problems were solved by two methods: (a) numerically suppressing the oscillations in the data, and (b) mechanically dampening the vibrations during testing.

A complex discrete Fourier transform, as follows, was applied to the data:

$$F(j) = \frac{1}{\sqrt{N}} \sum_{m=1}^{N} f(m) e^{(2\pi i(m-1)(j-1)/N)} \tag{15}$$

where $F(j)$ is element j of the transform, N is the number of data points, and $f(m)$ is element m of the data. Such a transform converts the data into a function of sines and cosines of varying frequency. The independent variable, j, is the frequency of the sines and cosines, while the dependent variable, $F(j)$, contains the complex coefficients of the sines and cosines. In Fig. 2a, the raw data from Fig. 1 are displayed after being transformed; the magnitude of the coefficients is graphed versus a dimensionless frequency of $2j/N$. As can been seen in Fig. 2a, the magnitude of the transformed data is greatest near zero. This low frequency part of the data is the smooth load–displacement signal from the fracture of the specimen. High frequency vibrations are seen in the 0.2 to 0.5 region of this dimensionless scale.

A low pass filter was used to remove the high frequency components while preserving the low frequency part of the data. An appropriately scaled Gaussian was used to generate a data set containing the same number of points as the load data; this Gaussian data set is referred to as a kernel. This kernel was transformed and multiplied by the transform of the raw data. Fig. 2b shows the result of applying the kernel. The low frequency elements have the same magnitude as in Fig. 2a, while the high frequency elements are essentially non-existent. An inverse Fourier transform of these data results in a smooth load–displacement curve (Fig. 1).

Unfortunately, this method was not effective for brittle fractures. For these samples, the load increases with displacement up to the failure and then drops suddenly to zero. Sharp transitions are not smooth and require high frequency components to be adequately represented. Applying the Fourier smoothing would result in these features being smoothed out. Because this method alone was applied to the tests with the neat SAN-g, and the blend with 40 wt% ABS, the peak load was estimated from the raw data for the samples of these materials which failed in a brittle manner.

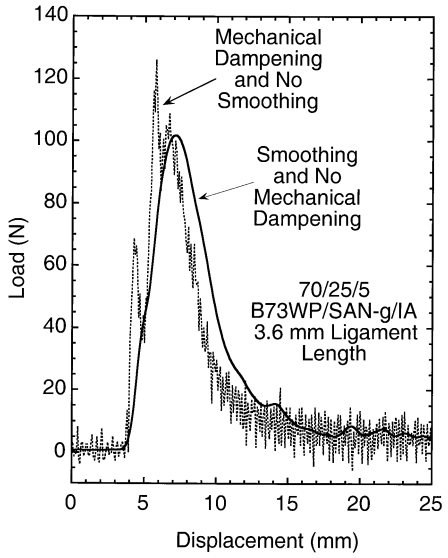

Fig. 3. Comparison of force-displacement data from a test with mechanical dampening at 25°C to data from an undampened test at 25°C but with Fourier smoothing for specimens of the 70/25/5 Capron B73WP/SAN-g/IA blend having ligament lengths of 3.6 mm.

Mechanical dampening (consisting of a rubber pad on the tup and rubber bands securing the sample ends to the testing frame) was used during the testing of the blend with 25 wt% ABS. A replicate set of data at 25°C was recorded without the use of the mechanical dampening; the numerical smoothing was applied to these data. Fig. 3 compares the two methods for samples, with similar ligament lengths, that fracture in a ductile manner. The Fourier method generated smoother load–displacement curves than did the rubber dampening. However, the mechanical dampening did not remove the sharp transitions at brittle failure. For the samples in Fig. 3, the peak load and energy were roughly the same from both methods. Differences in the results of the damped and undamped tests will be discussed in more detail later.

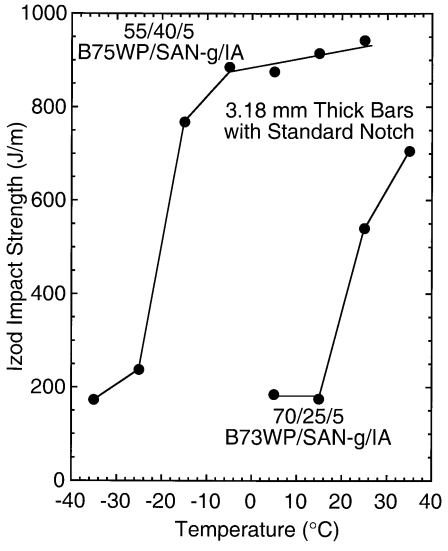

Fig. 4. Effect of temperature on Izod impact (standard notched) strength using 3.18 mm thick bars for 55/40/5 and 70/25/5 Capron B73WP/SAN-g/IA blends.

3. Results and Discussion

3.1. Notched Izod impact strength and morphology of the blends

Fig. 4 shows the standard notched Izod impact strength versus temperature for the blends with 25 and 40 wt% ABS. In this test, ductile fracture resulted in the samples being only partially fractured. The 40 wt% ABS blend has a room temperature Izod impact strength of 940 J/m and a ductile–brittle transition temperature of −20°C, while the 25 wt% ABS blend shows values of 540 J/m and 25°C, respectively. The Izod impact strength in the brittle region was about 200 J/m for both blends.

Fig. 5 shows transmission electron micrographs of the two blends; phosphotungstic acid (PTA) staining causes the nylon phase to appear dark. In both cases, nylon 6 is the continuous phase; however, the blend with 40 wt% ABS is close to the phase inversion point, so there is a tendency for phase co-continuity. The 25 wt% ABS blend is much further in composition from the co-continuous region. In both cases, the ABS domains are reasonably small and well dispersed.

3.2. Temperature–ligament length fracture maps for the drop tower tests

Depending on the temperature and ligament length, the various materials show different fracture behavior in the three point bend test, which is mapped onto plots of ligament length versus temperature. The neat ABS material fractures in a ductile manner at all temperatures and ligaments lengths; thus, no fracture map is shown for this system. In contrast, both nylon 6/ABS blends show three types of fracture: (a) fully ductile fracture; (b) mixed mode fracture — ductile yield followed by brittle fracture (as evidenced by both the shape of the load–displacement curves and a region of stress whitening at the notch followed by a region of no stress whitening as the crack extended), and (c) fully brittle fracture.

As seen in Fig. 6, at 25°C, the blend containing 40 wt% ABS fractures in a ductile manner for all ligament lengths; while at 15 and 5°C, some of the specimens with longer ligaments fail in the mixed mode. At −5°C and lower, some of the samples having long ligament lengths fractured in a brittle manner. A boundary (solid line) was identified which roughly separates the ductile fractures from the two types of brittle fracture. The dashed curve is formed by the ligament length criterion in Eq. (9), using the flexural yield stress and the critical stress intensity factors calculated from the

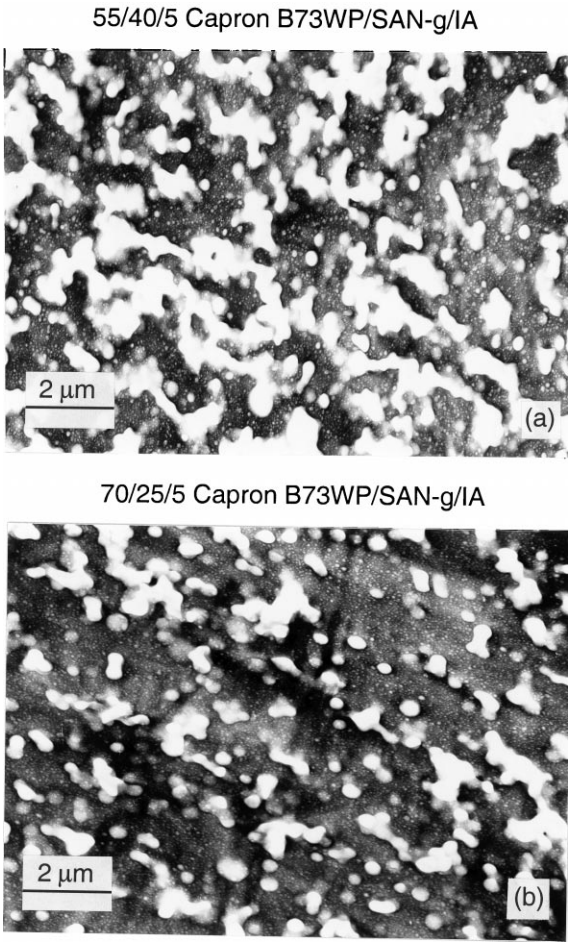

Fig. 5. TEM photomicrographs showing the morphology of: (a) the 55/40/5 and (b) the 70/25/5 Capron B73WP/SAN-g/IA blends; the nylon 6 phase is stained dark with phosphotungstic acid.

tests. This curve falls slightly below the measured ductile–brittle ligament length transition. At −20°C, the ductile–brittle transition temperature as determined by the Izod test, ductile fracture still occurs when ligament lengths are less than 5.5 mm.

The ligament length fracture map is shown in Fig. 7 for the blend containing 25 wt% ABS. Only the results from the tests using the mechanical dampening are shown. In this system, the region of ductile fracture is much smaller. All fractures are brittle, at −15°C and below. At room temperature (which is the ductile–brittle transition temperature by the Izod test), all three modes of fracture are observed, with a transition from ductile to brittle fracture occurring at a ligament length of approximately 7.7 mm. Again the dashed line is from the ligament length criterion in Eq. (9). This criterion underestimates the transition ligament length at temperatures of 25–0°C and overestimates the transition from temperatures of 0– − 25°C. Overall this criterion captures the transition reasonably well for both of these blends.

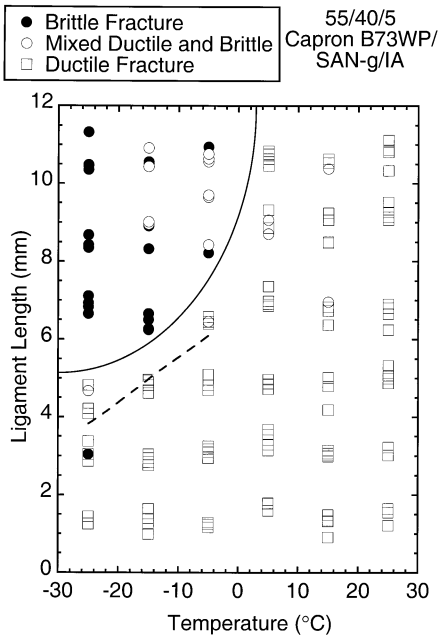

Fig. 6. Map of the fracture for the 55/40/5 Capron B73WP/SAN-g/IA blend obtained in the three point bend test. Solid line is the measured ductile–brittle transition ligament length. Dashed line is $l = 2.5\ (K_{IC}/\sigma_y)^2$.

3.3. Essential work of fracture analysis

Specific fracture energy is plotted versus ligament length for the neat ABS (SAN-g) in Fig. 8 (only data at 25, 5, and −25°C are shown). All of the SAN-g specimens fractured in a ductile manner (i.e. at all ligament lengths and temperatures). The essential work of fracture parameters, u_d and u_o,

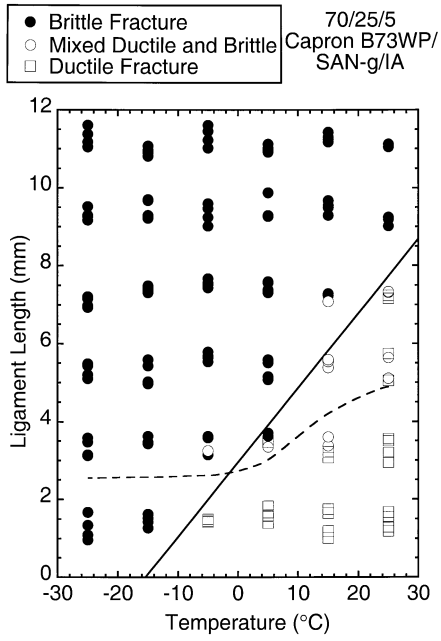

Fig. 7. Map of the fracture types for the 70/25/5 Capron B73WP/SAN-g/IA blend obtained in the in three point bend test. Solid line is the measured ductile–brittle transition ligament length. Dashed line is $l = 2.5\ (K_{IC}/\sigma_y)^2$.

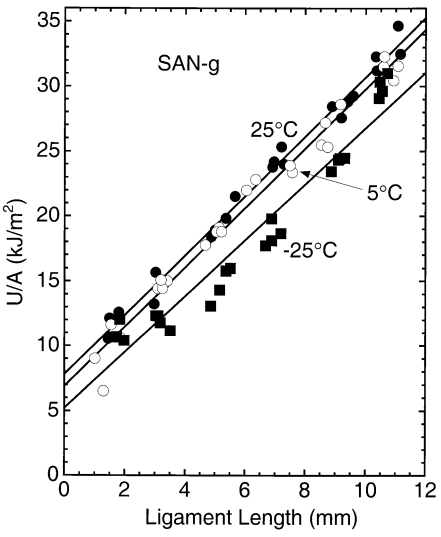

Fig. 8. Effect of temperature on specific fracture energy and fit of the essential work of fracture (EWF) model for neat ABS.

are listed in Table 2. Overall, the specific fracture energy decreases slightly as the temperature is reduced. The scatter in the data also increases as temperature is decreased. In addition, the specific fracture energies tend to fall slightly below the regression lines from a ligament length of 4 to 10 mm below −5°C, but above the line for ligament lengths less than 3 or greater than 11 mm, i.e. a slight curvature exists. Both the scatter and the curvature affects the fit of u_o and u_d, as reflected in the uncertainties for these parameters at the lower temperatures (see Table 2).

Even though great care was taken to ensure precise temperature control of the samples, the control was less precise as temperature decreased in part due to some warming during the transfer of the specimens from the cooling chamber to the testing frame. This may explain the scatter in the data at the low temperatures. The crack initiation and propagation in the warmer volume of the sample, near the surface, may have resulted in the specific fracture energy being slightly increased, for samples with long or short ligament lengths. Samples with ligament lengths in the mid-range are expected to be less affected by warming, causing these fracture energies to have a larger dependence on the reported test temperature. A failure to satisfy the ligament length and yielding criteria of the EWF model may also contribute to the curvature; a lower temperature may make the effects more pronounced.

Table 2
Effect of temperature on the fracture parameters for SAN-g

Temperature (°C)	u_d (MJ/m^3)	u_o (kJ/m^2)	σ_y (MPa)
25	2.29 ± 0.10	7.80 ± 0.73	34
15	2.45 ± 0.12	6.62 ± 0.85	36
5	2.29 ± 0.14	6.88 ± 0.99	36
−5	2.01 ± 0.12	7.87 ± 0.82	35
−15	2.07 ± 0.23	6.7 ± 1.6	36
−25	2.15 ± 0.23	5.2 ± 1.6	36

Both brittle and ductile fractures were observed for the blend containing 40 wt% ABS. The critical strain energy release rate model was fitted to the brittle fracture energies. The kinetic energy correction in the G_{IC} model is essentially the same for all specimens and is approximated to be the translational kinetic energy of the sample at the testing speed (0.027 J). This term is the intercept in a plot of fracture energy versus $tW\phi$, while the critical strain energy release rate is the slope (see Fig. 9a for the regression at −25°C). The essential work of fracture model was fitted to the ductile-fracture energies. Examples of both models for this blend are shown in a plot of specific fracture energy versus ligament length in Fig. 9b; at 25 and 5°C, only the EWF model is applied, while at −25°C both models are applied. It can be seen that the EWF model provides an excellent representation of the ductile-fracture energies, while the critical strain energy release rate model gives an excellent fit of the brittle-fracture energies. The EWF parameters and the G_{IC} values are listed in Table 3 for all temperatures.

A reduction in the specific fracture energy occurs as temperature is decreased, for the samples which fractured in a ductile manner (see Fig. 9b). However, the transition from ductile to brittle fracture (controlled by both temperature and ligament length) leads to a dramatic decrease in the specific fracture energies. For example, two samples fractured in a mixed mode at 5°C and have specific fracture energies of about half those of specimens fracturing in a ductile manner at comparable ligament lengths. At −25°C, the transition to brittle fracture occurs at a ligament length of about 5 mm; the dashed line shows the transition from the application of the EWF model to the G_{IC} model. The specific brittle-fracture energy is essentially constant at about 5 kJ/m^2 (at −25°C) from ligament lengths of 6 to 9 mm, but increases from ligament lengths of 9 to 12 mm. This increase is predicted by the G_{IC} model as a result of the non-linearity of the factor ϕ with ligament length.

The essential work of fracture model predicts a constant specific fracture energy, i.e. $u_d = 0$ and u_o = constant, for brittle fractures. The increase in specific fracture energy observed at long ligament lengths is probably due to the fact that the samples used in this study do not satisfy the ligament length criterion in that model and possibly do not satisfy the yielding criterion [12]. The EWF model provides a good description of the ductile-fracture energies; but it cannot be applied successfully to the brittle-fracture energies of specimens with this geometry and range of ligament lengths. However, the entire range of behavior is modeled in a quantitative manner by applying each model over the appropriate range.

The 25 wt% ABS blend specimens fail more frequently in a brittle manner. As a result, EWF parameters could be obtained only at 25, 15, and 5°C, while G_{IC} values were determined at all temperatures, see Table 4. The specific

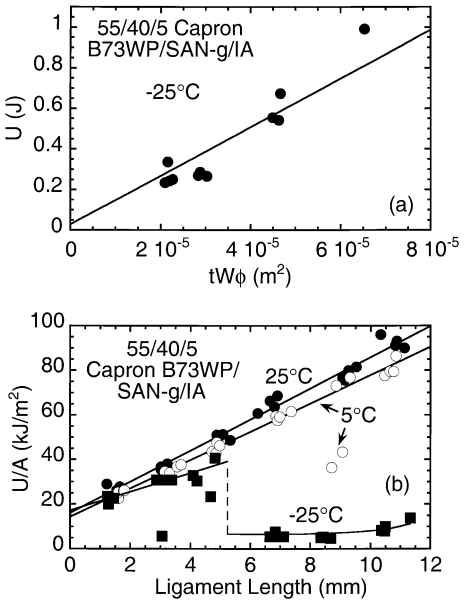

Fig. 9. (a) Fit of the fracture data for the 55/40/5 Capron B73WP/SAN-g/IA blend at −25°C to the G_{IC} model. (b) Effect of temperature on specific fracture energy and fit of the EWF and G_{IC} models for this blend. Solid line drawn in part (b) for −25°C and $l > 5$ mm is the same as the solid line in part (a).

fracture energy versus ligament length is shown in Fig. 10 for the test at 25°C, in which the mechanical dampening was used. In comparison, Fig. 11 shows results from the test at the same temperature when no dampening was used. As in the previous case, the G_{IC} model is fitted to the specific brittle-fracture energies, while the EWF model is fitted to the specific ductile-fracture energies. In Figs. 10 and 11, both models are shown over the appropriate ranges.

The specific energies for the ductile fractures are essentially the same with and without dampening, such that the differences in slopes and intercepts are not statistically significant. However, the transition to brittle fracture occurs with a ligament length of approximately 8 mm in the test in which dampening was used and at about 5 mm without dampening. The specific fracture energies of the brittle samples span from 9 to 16 kJ/m^2 ($G_{IC} = 15$ kJ/m^2) when dampening was used and 4–9 kJ/m^2 ($G_{IC} = 8.4$ kJ/m^2) when dampening was not used. In addition, four samples fractured in the mixed mode in the test in which dampening was used, while none did so in the test without dampening.

A few factors can be sited that may help to explain these differences. As seen in Fig. 1, the load sensed by the tup is occasionally negative during the test; however, the tup and the sample are not coupled in a manner such that a negative load on the sample is physically possible, which means that the tup is vibrating or ringing during the test. As a result, the sample experiences a cyclic load because of the contact with the tup, albeit not exactly that which is measured by the force transducer. Mechanical dampening results in a great reduction in the vibrations recorded during the test (Fig. 3) and thus reduces the amount of cyclic load experienced by a test specimen. In addition, the initial loading rate of a sample is slower with mechanical dampening because of the compression of the rubber pad during loading. Both of these differences would tend to increase the energy of brittle or mixed mode fracture and shift the ligament length at which the transition occurs to higher values when dampening is used.

The results from a test of the same blend at −25°C (mechanical dampening used) are depicted in Fig. 12a and b. In this test, all of the samples failed in a brittle manner. Fig. 12a shows the regression of the critical strain energy release rate model to the data where $a/W \leq 0.6$. Fig. 12b displays all of the data (i.e. for all notch depths) graphed as specific fracture energy versus ligament length; the solid line was calculated from the G_{IC} model fit in Fig. 12a. When shown in this manner, it is obvious that the high testing rate (3.4 m/s) causes the kinetic energy contribution to be a significant part of the fracture energy at ligament lengths less than 2 mm. As the ligament length increases from 2 mm, the kinetic energy contribution is constant while the total fracture energy increases proportional to fracture area. This results in a slight negative slope in specific energy versus ligament length at intermediate ligament lengths (2–10 mm). Even though the data from samples with ligament lengths less than 5.1 mm were not used to determine the G_{IC} value (because of the criterion), the model still accurately represents these data. The significant increase in specific fracture energy at long ligament lengths observed previously is also observed for these specimens.

The effect of temperature on the specific fracture energy is dependent on the ligament length. Fig. 13 shows specific fracture energy versus temperature at three ligament lengths for the 40 wt% ABS blend. In general, the specific fracture energy decreases as the temperature is reduced; however,

Table 3
Effect of temperature on the fracture parameters for the 55/40/5 capron B73WP/SAN-g/IA blend

Temp. (°C)	u_d (MJ/m^3)	u_o (kJ/m^2)	G_{IC} (kJ/m^2)	σ_y (MPa)	K_{IC} (MPa m$^{1/2}$)
25	6.99 ± 0.38	16.0 ± 2.6	–	86	–
15	6.10 ± 0.10	8.6 ± 3.2	–	87	–
5	6.36 ± 0.28	14.3 ± 1.8	–	88	–
−5	5.65 ± 0.53	14.8 ± 2.2	19	88	4.3
−15	4.66 ± 0.72	17.0 ± 2.4	15	87	3.9
−25	4.2 ± 1.3	16.9 ± 3.9	12	97	3.4

Table 4
Effect of temperature on the fracture parameters for the 70/25/5 Capron B73WP/SAN-g/IA blend (only (a) was determined using Fourier smoothing and no mechanical dampening; all other data were taken using mechanical dampening)

Temp. (°C)	u_d (MJ/m^3)	u_o (kJ/m^2)	G_{IC} (kJ/m^2)	σ_y (MPa)	K_{IC} (MPa m$^{1/2}$)
25[(a)]	3.0 ± 4.9	13 ± 19	8.4	88	3.0
25	4.64 ± 0.80	9.6 ± 3.4	15	95	4.2
5	3.8 ± 1.8	10.4 ± 3.9	11	91	3.9
5	3.2 ± 3.2	11 ± 7	9.0	100	3.3
−5	–	–	7.1	93	3.0
−15	–	–	6.7	–	3.1
−25	–	–	6.0	–	2.9

for the longer ligament lengths (10.7 and 6.6 mm), a transition to brittle fracture occurs causing the energy to drop abruptly to about 10 kJ/m^2. For the shortest ligament length, no transition to brittle fracture occurs. The slope of fracture energy versus temperature becomes greater as ligament length is increased.

The essential work of fracture parameters u_d and u_o are shown as a function of temperature in Figs. 14 and 15 for the neat ABS (i.e. SAN-g) and the 40 wt% ABS blend, respectively. For the neat ABS, both u_d and u_o decrease approximately linearly with decreasing temperature. For the 40 wt% ABS blend, u_d decreases with a reduction in temperature in a roughly linear fashion, while u_o is essentially constant. The uncertainties in u_d and u_o are large for the 25 wt% ABS blend; however, u_d clearly decreases with decreasing temperature, while u_o seems to be constant (Table 3). Thus, as temperature decreases, the ability of a specimen to dissipate energy by plastic work (indicated by u_d) decreases. The 40 wt% ABS blend has the highest values of u_d and u_o, followed by the 25 wt% ABS blend, and with the neat ABS having the smallest values for both u_d and u_o. For comparison, the values for neat nylon 6 are as follows: $u_d = 0$, $u_o = 7.2$ kJ/m^2 [12].

Fig. 16 shows that as temperature is reduced from 25°C, G_{IC} decreases steeply and then less so at lower temperatures, for the 25 wt% ABS blend. As seen in Table 3, G_{IC} also apparently decreases with a reduction in temperature for the 40 wt% ABS blend, based on the three data points available. The critical stress intensity factor, discussed in the next section, shows an analogous trend. Similar behavior of K_{IC} and G_{IC} has also been reported by others [38–41]. It seems reasonable, that during brittle fracture at 25°C, these specimens are able to deform plastically around the crack tip before the initiation of the crack extension. As the temperature is decreased, less deformation of this type can occur, with the result that the failure stress and fracture energy decrease. At a sufficiently low temperature, this plastic deformation becomes almost insignificant; hence, the failure stress and, thus, K_{IC} and G_{IC} become relatively insensitive to temperature. A visual inspection of the fracture surfaces supports this conclusion. The zone of stress whitening at the sharp notch decreased in size from 25

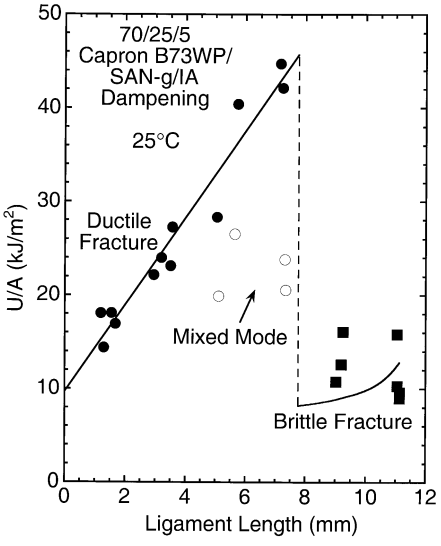

Fig. 10. Fit of the essential work of fracture (EWF) model to the specific fracture energy for the 70/25/5 Capron B73WP/SAN-g/IA blend at 25°C (mechanical dampening used) for samples that failed in a ductile manner ($l < 8$ mm). Solid line drawn for $l > 8$ mm is from the G_{IC} model.

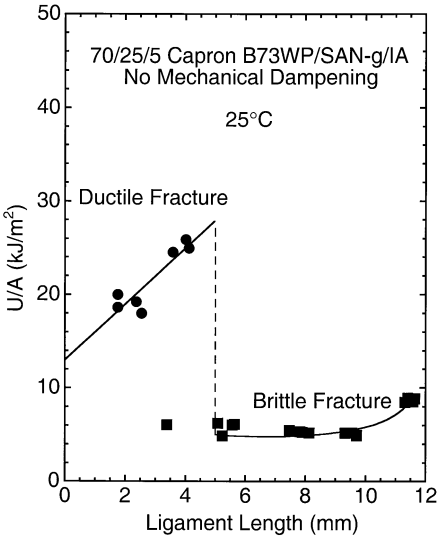

Fig. 11. Fit of the essential work of fracture (EWF) model to the specific fracture energy for the 70/25/5 Capron B73WP/SAN-g/IA blend at 25°C (mechanical dampening not used) for samples that failed in a ductile manner ($l < 5$ mm). Solid line drawn for $l > 5$ mm is from the G_{IC} model.

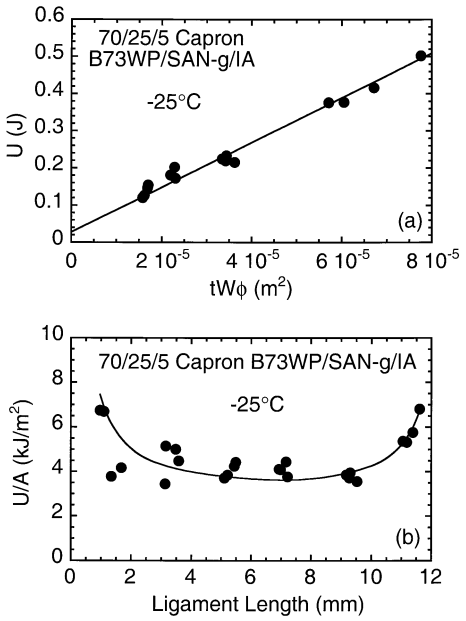

Fig. 12. (a) G_{IC} regression for the 70/25/5 Capron B73WP/SAN-g/IA blend at −25°C.(b) Replot of the data in part (a) in the form of specific fracture energy versus ligament length (i.e. EWF form); solid line drawn is the same as solid line in part (a).

to −5°C; at −5°C and lower, the zone was almost non-existent.

3.4. Analysis of the yield stress and critical stress intensity factor

The yield stress, σ_y, characterizes the load required to cause ductile fracture, while the plane-strain critical stress intensity factor, K_{IC}, characterizes the load required to cause brittle fracture. Here, the failure stress was calculated from the peak load of the force-displacement data. Samples which failed in the mixed mode are grouped together with samples that fractured in a ductile manner, because the specimens yielded in both cases. The models for σ_y and K_{IC} are fit to the failure stresses using non-linear regression.

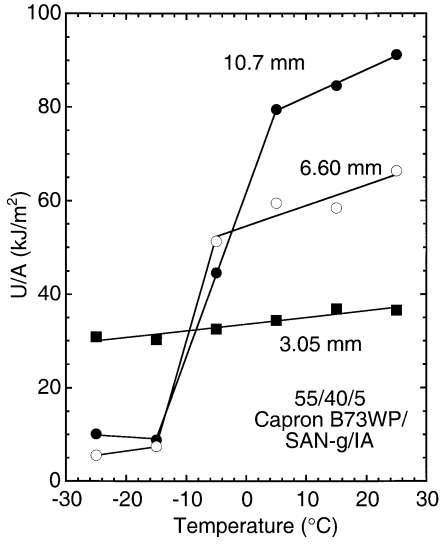

Fig. 13. Effect of temperature on specific fracture energy for samples of the 55/40/5 Capron B73WP/SAN-g/IA blend with ligament lengths of 10.7, 6.60, and 3.05 mm.

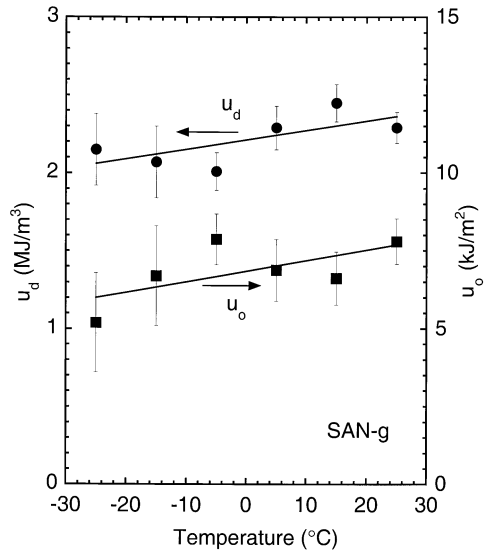

Fig. 14. Effect of temperature on the EWF parameters u_o and u_d for neat ABS.

Figs. 17a and b show the failure stress for the neat ABS at 25°C and −25°C, respectively. It should be noted that the σ_y model fits the failure stresses extremely well at most ligament lengths. Because all of the neat ABS samples fractured in a ductile manner, K_{IC} regression was not possible. From Table 2 it is seen that the yield stress calculated from the data is essentially independent of temperature which is an unexpected result. The yield stress, when measured directly,

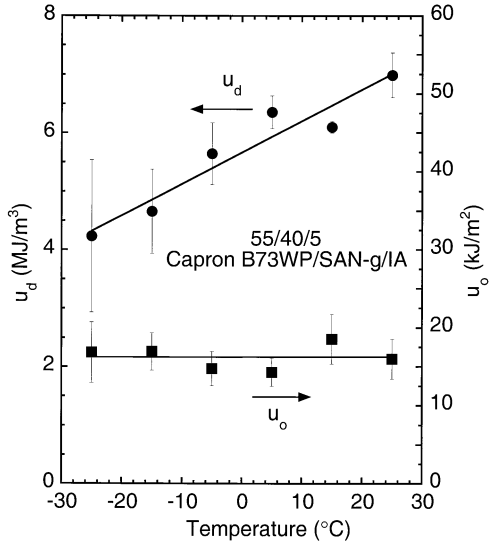

Fig. 15. Effect of temperature on the EWF parameters u_o and u_d for the 55/40/5 Capron B73WP/SAN-g/IA blend.

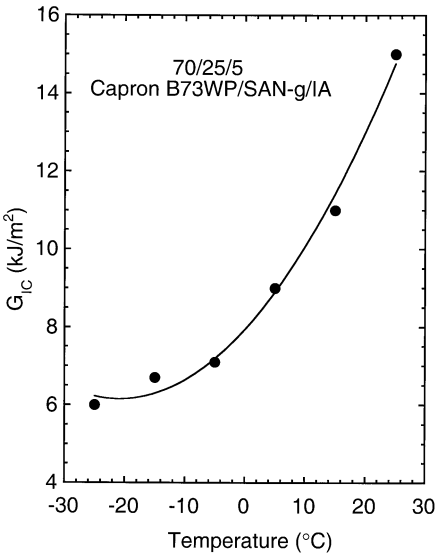

Fig. 16. Effect of temperature on G_{IC} for the 70/25/5 Capron B73WP/SAN-g/IA blend.

decreases significantly as temperature is increased [39,42–48]. However, it is typically measured with unnotched specimens and occasionally with standard notch specimens. Kitagawa and Yammaura demonstrated that reducing the notch radius of a three point bend specimen from 2 to 0.25 mm significantly reduces the temperature dependence of the yield stress for both polycarbonate and polypropylene and explain this result in plane-strain with a slip line field analysis [49,50]. Although the ABS did not fracture in plane strain, a similar effect seems reasonable; the sharp notches in the samples probably greatly reduce the temperature dependence of the yield stress.

Brittle fracture occurs at some ligament lengths for the blend containing 40 wt% ABS, allowing both models to be fit to these data (Figs. 17c and d and Table 3). The same trend is observed in σ_y as with the neat ABS; it is essentially constant with decreasing temperature. For −25°C, the yield stress is larger than at any of the previous temperatures. However, the failure stresses of the specimens with short ligaments tended to fall slightly above the curve fit for σ_y. Only the samples with short ligament lengths fail in a ductile manner at −25°C, which results in an inflated value of the yield stress at this temperature. A comparison of Fig. 17d with 17c demonstrates that the values for the failure stresses are essentially the same. The critical stress intensity factor appears to decrease as temperature is reduced (for three temperatures).

Fig. 17e shows the failure stress at 25°C for the 25 wt% ABS blend determined from tests using rubber dampening and from tests without mechanical dampening. The failure stresses for the samples which fractured in a ductile manner are slightly higher when dampening was used than when it was not used. This difference is not pronounced but results in slightly higher yield stresses when dampening was used (see Table 4). A larger difference in the failure stresses is observed for samples which failed in a brittle manner; the use of dampening results in a significantly larger failure stress. Figs. 10 and 11 show a similar trend in the specific fracture energies. As discussed in the previous section, the use of rubber dampening reduces the loading rate and degree of cyclic load that is experienced by the sample; which results in an increase in both the failure stress and the fracture energy of a sample which fails in a brittle manner.

The failure stresses for the same material at −25°C are shown in Fig. 17f; at this temperature, all of the specimens failed in a brittle manner. Note that this test was performed with the use of rubber dampening. The yield stress of this blend is also essentially independent of temperature (Table 4). In contrast, the critical stress intensity factor decreases as the temperature is lowered from 25 to −5°C, similar to the result with the 40 wt% ABS blend; from −5 to −25°C, K_{IC} is nearly constant. This result is explained in the previous section.

The invariance of σ_y with temperature for all three of the materials examined provides insight into the effect of temperature on the ductile fracture of these materials. An examination of the load–displacement curves from specimens with similar ligament lengths, over a range of temperatures, revealed that the loading part of the curves (i.e. from the initial impact of the tup with the sample to the yield point) are essentially identical. The crack propagation part of the curves (at displacements past the yield point) on the other hand, are quite different. As temperature is reduced, the load in this part of the curve decreases. This post-yield difference is the cause of the decrease in fracture energy as temperature is reduced. Thus, neither the modulus nor the yield stress is significantly affected by temperature for the samples that fracture in a ductile manner.

Fig. 18 shows G_{IC} versus K_{IC}^2 for (a) the 40 wt% ABS blend and (b) the 25 wt% ABS blend. From Eq. (14), the slopes of these plots, 1.0 GPa^{-1} in (a) and 0.78 GPa^{-1} in (b), should be $(1-\nu^2)/E$. The exact values of ν and E are not available for these materials under the testing conditions. The tensile modulii measured at 25°C and a testing rate of 5.08 mm/min are 1.6 GPa for the 40 wt% ABS blend and 1.9 GPa for the 25 wt% ABS blend [51]. As a cross-check, Poisson's ratio is assumed to be 0.3, and the modulii of these materials are calculated from these slopes to be 0.91 GPa for the 40 wt% ABS blend and 1.2 GPa for the 25 wt% ABS blend (40% deviation from the measured tensile modulus in both cases). Therefore, the slopes in the plots in Fig. 18 are larger than $(1-\nu^2)/E$, which indicates a discrepancy between the K_{IC} and the G_{IC} values. Any deviations from pure linear elastic behavior would affect the slopes in these plots. In addition, the compliances, for which no correction was made, may have caused the values for G_{IC} to be inflated. The European Structural Integrity Society (ESIS) protocol, recommends not using Eq. (14) to check accuracy, because of the difficulty in accurately determining the specimen compliance at testing rates over 1 m/s [36].

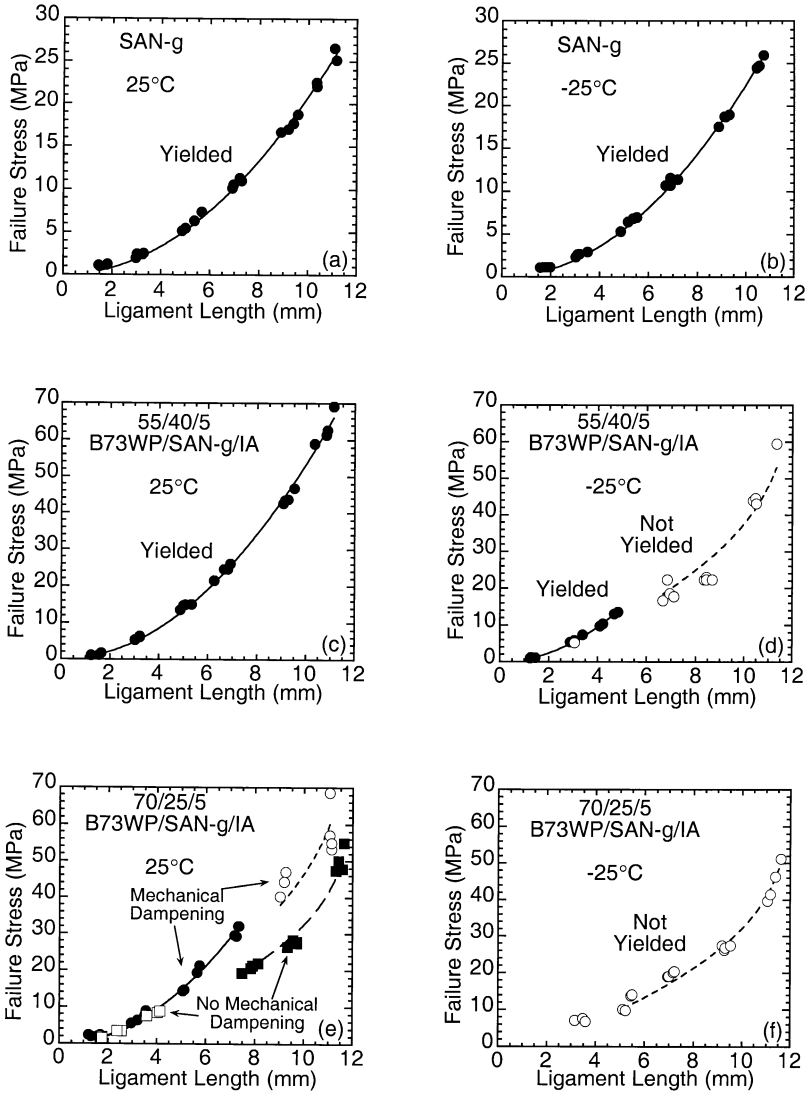

Fig. 17. Effect of temperature on the failure stress and fits of the yield stress model to the ductile-failure stress and the K_{IC} model to the brittle-failure stress for the ABS, the 55/40/5, and the 70/25/5 Capron B73WP/SAN-g/IA blends.

4. Conclusions

An essential work of fracture technique was used in conjunction with the critical strain energy release rate model to further illuminate the ductile–brittle transition behavior of neat ABS and blends containing 40 and 25 wt% ABS. The effect of composition, temperature, and ligament length on the transition was examined using three point bend specimens with sharp notches in an instrumented drop tower test. Three modes of fracture were observed: (a) ductile fracture; (b) mixed mode; and (c) brittle fracture.

The EWF model was fitted to the specific ductile-fracture energies. For the three materials studied, the dissipative energy density, u_d, was found to decrease as the temperature was reduced. In the neat ABS, the limiting specific fracture energy, u_o, also decreased with decreasing temperature, while for the two blends, u_o was found to be essentially constant. The G_{IC} model with a kinetic energy correction was fitted to the brittle-fracture energies. The specific brittle-fracture energy was found to decrease with ligament length at short ligament lengths as a result of kinetic energy effects. The specific brittle-fracture energy increased with ligament length at long ligament lengths. The critical strain energy release rate model was found to represent these trends in a quantitative manner. By applying the EWF model to the ductile-fracture energies and the critical strain energy release rate model to the brittle-fracture energies, the entire range of behavior is captured quantitatively.

By fitting a model for yielding to the failure stress data for ductile fractures, it was observed that the yield stress, σ_y, was essentially constant over this temperature range at this testing speed (3.4 m/s). A possible explanation, supported by the literature, is that the sharp notches used in this study result in the yield stress being essentially invariant over the temperature range studied. By fitting a critical stress intensity factor model to the failure stress of samples that failed

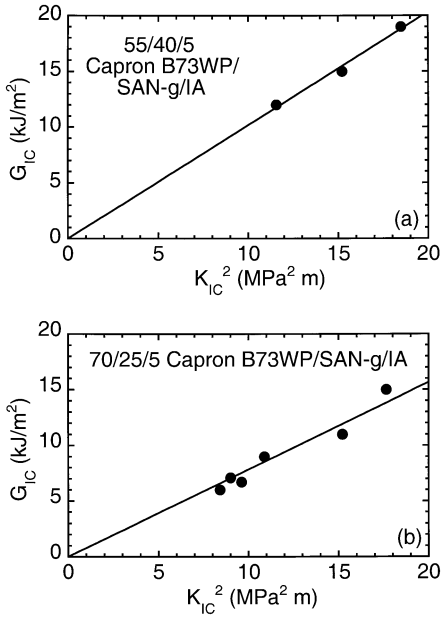

Fig. 18. Comparison of the values of G_{IC} and K_{IC} for: (a) the 55/40/5 Capron B73WP/SAN-g/IA blend; (b) the 70/25/5 Capron B73WP/SAN-g/IA blend.

in a brittle manner, it was found that K_{IC} decreased initially, then remained at a fairly constant value as temperature was lowered. Similar behavior was observed for values of the critical strain energy release rate. Apparently, less plastic deformation occurs at the notch prior to crack extension as temperature is reduced, which in turn reduces the failure stress.

Acknowledgements

The authors thank AlliedSignal, Cheil Industries, and Rohm and Haas for donating materials.

References

[1] Otterson DM, Kim BH, Lavengood RE. J Mater Sci 1991;26:1478–84.
[2] Otterson DM, Kim BH, Lavengood RE. J Mater Sci 1991;26:4855–60.
[3] Triacca VJ, Ziaee S, Barlow JW, Keskkula H, Paul DR. Polymer 1991;32:1401–13.
[4] Aoki Y, Watanabe M. Polym Engng Sci 1992;32:878–85.
[5] Kim BK, Lee YM, Jeong HM. Polymer 1993;34:2075–80.
[6] Misra A, Sawhney G, Kumar RA. J Appl Polym Sci 1993;50:1179–85.
[7] Majumdar B, Keskkula H, Paul DR. J Polym Sci, Part B: Polym Phys 1994;32:2127–33.
[8] Majumdar B, Keskkula H, Paul DR. Polymer 1994;35:5468–78.
[9] Majumdar B, Keskkula H, Paul DR. Polymer 1994;35:5453–67.
[10] Wong SC, Nair SV, Vestergaard LH. Plastics Engng 1995;51:23–4.
[11] Lee CW, Ryu SH, Kim HS. J Appl Polym Sci 1997;64:1595–604.
[12] Kudva RA, Keskkula H, Paul DR. Polymer 2000;41:335–49.
[13] Broberg KB. Int J Fract Mech 1968;4:11–7.
[14] Vu-Khanh T. Polymer 1988;29:1979–84.
[15] Saleemi AS, Nairn JA. Polym Engng Sci 1990;30:211–8.
[16] Mai Y-W, Powell P. J Polym Sci, Part B: Polym Phys 1991;29:785–93.
[17] Chan WYF, Williams JG. Polymer 1994;35:1666–72.
[18] Karger-Kocsis J, Czigany T. Polymer 1996;37:2433–8.
[19] Wu J, Mai YM. Polym Engng Sci 1996;36:2275–88.
[20] Levita G, Parisi L, Marchetti A, Bartolommei L. Polym Engng Sci 1996;36:2534–41.
[21] Karger-Kocsis J, Czigany T, Moskala EJ. Polymer 1997;38:4587–93.
[22] Pegoretti A, Marichi A, Ricco T. Polym Engng Sci 1997;37:1045–52.
[23] Kayano Y, Keskkula H, Paul DR. Polymer 1998;39:821–34.
[24] Karger-Kocsis J, Czigany T, Moskala EJ. Polymer 1998;39:3939–44.
[25] Liu C-H, Nairn JA. Polym Engng Sci 1998;38:186–93.
[26] Ferrer-Balas D, Maspoch ML, Martinez AB, Santana OO. Polym Bull 1999;42:101–8.
[27] Casellas JJ, Frontini PM, Carella JM. J Appl Polym Sci 1999;74:781–96.
[28] Mouzakis DE, Karger-Kocsis J. Polym Bull 1999;42:473–80.
[29] Mai Y-M. Int J Mech Sci 1993;35:995–1005.
[30] Wong S-C, Mai Y-M. Polym Engng Sci 1999;39:356–64.
[31] Santana OO, Maspoch ML, Martínez AB. Polym Bull 1997;39:511–8.
[32] Standard test methods for plane-strain fracture toughness and strain energy release rate of plastic materials. D5045-99, ASTM, 1999.
[33] Okada O, Keskkula H, Paul DR. Polymer 2000;41:8061–74.
[34] McCrum NG, Buckley CP, Bucknall CB. Principles of polymer engineering. New York: Oxford University Press, 1988 (chap. 5).
[35] Brown WF, Srawley JE. Plane strain crack toughness testing of high strength metallic materials. STP 410, Baltimore: ASTM, 1966.
[36] A linear elastic fracture mechanics (LEFM) standard for determining K_{IC} and G_{IC} for plastics at high loading rates. FR177, ESIS, 1996.
[37] Standard test methods for determining the izod pendulum impact resistance of plastics. D256-97, ASTM, 1997.
[38] Plati E, Williams JG. Polymer 1975;16:915–20.
[39] Parvin M, Williams JG. J Mater Sci 1976;11:2045–50.
[40] Mizutani K, Yoshii M. J Mater Sci 1998;23:3501–4.
[41] Low M-I, Mai Y-W. J Mater Sci 1989;24:1634–44.
[42] Parvin M, Williams JG. J Mater Sci 1975;10:1883–8.
[43] Mizutani K. J Mater Sci Lett 1987;6:915–6.
[44] Ikeda RM. J Appl Polym Sci 1993;47:619–29.
[45] Chang F-C, Hsu H-C. J Appl Polym Sci 1994;52:1891–904.
[46] Hamdan S, Swallowe GM. J Mater Sci 1996;31:1415–23.
[47] Gaymans RJ, Hamberg MJJ, Inberg JPF. Polym Engng Sci 2000;40:256–62.
[48] Lee SI, Chun BC. J Mater Sci 2000;35:1187–93.
[49] Kitagawa M. J Mater Sci 1982;17:2514–24.
[50] Kitagawa M, Yammaura H. J Mater Sci 1984;19:1863–75.
[51] Kudva RA, Keskkula H, Paul DR. Polymer 2000;41:225–37.